

Torqued Accelerator using Radiation from the Sun (TARS) for Interstellar Payloads

DAVID KIPPING¹ AND KATHRYN LAMPO¹

¹*Columbia University, 550 W 120th Street, New York NY 10027*

ABSTRACT

The concept of exploring space using solar power is energetically appealing, but interstellar solar sails typically require extremely low areal densities ($\sim 0.8 \text{ g/m}^2$). This work explores an alternative approach: storing solar energy as rotational kinetic energy, which is later released to propel a microprobe beyond the solar system. The proposed Torqued Accelerator using Radiation from the Sun (TARS) consists of two thin surfaces with contrasting albedos that gradually spins up over weeks to months while in a sub-Keplerian “quasite” orbit around the Sun. Though constrained by material strengths, careful design allows a phone-sized payload to reach interstellar velocities in less than a year, using commercially available materials (e.g. CNT sheets). The entire system spans tens of meters and weighs of order of a kilogram. Whilst there is no theoretical limit to the achievable speeds, practical designs grow exponentially in size as velocity targets increase, making interstellar flight feasible but relativistic speeds implausible. Several strategies, including the use of graphene sheets, gravity assists, the Oberth effect, and electrostatic confinement, could further maximise velocity. TARS is an attractive light sail technology when high-powered directed energy systems are impractical, offering a potentially low-cost solution for deploying small, sub-relativistic interstellar probes.

Keywords: interstellar propulsion — solar sails

1. INTRODUCTION

Light sails have long been recognised as a potential means of exploring our solar system and beyond, powered either by natural solar radiation or directed energy systems (Zander 1964; Forward 1984; Marx 1966; Redding 1967; Moeckel 1972; Weiss et al. 1979). An intrinsic benefit of light sails is that the fuel needed for propulsion need not be carried onboard the spacecraft, freeing the vessel from the so-called “tyranny of the rocket equation” (Tsiolkovsky 1968). On the other hand, this advantage is ostensibly intertwined with a disadvantage - radiation pressure always acts in a di-

rection pointing radially away from the energy source (Lebedev 1901; Nichols & Hull 1903). Consequently, the spacecraft will have an acceleration vector pointing *away* from the source (barring other forces), ultimately leading to a drop off in radiation pressure.

Certainly light sails can move towards the light source, thereby increasing their incident radiation pressure, but they will be decelerating during such motion and will eventually reverse and accelerate away. An exception to this can occur for solar sails in orbit of the Sun (or indeed some other star), where they can use angled reflectors to induce forces tangential to their orbital motion, thus allowing them to transfer to inner (or outer) orbits (Powers & Coverstone 2001).

Depending upon such transfer orbits for an interstellar light sail is not ideal, as the transfer time is of order of the longest orbital period of the two orbits (Powers & Coverstone 2001), thus taking centuries to reach the Kuiper belt for example (and technically infinite time to reach interstellar space). Another option might be to simply direct one's solar sail outwards, but the Sun's gravitational force will usually dwarf that of radiation pressure unless the sail is exceptionally light.

To see this, consider the simple case of a solar sail at rest at some radial distance r_i from the Sun. The inward acceleration due to the Sun's gravity is GM_\odot/r_i^2 , whereas the idealised outward radiation force is $L_\odot/(4\pi c\Sigma r_i^2)$ (if normal to the Sun). Accordingly, an interstellar solar sail would require a mass-per-unit-area of $\Sigma \leq L_\odot/(4\pi cGM_\odot) = 0.77 \text{ g m}^{-2}$ for direct radial escape.

The problem of how to get a light sail to leave our solar system is well-recognised, and much research effort has been focussed on the idea of directed energy systems (Marx 1966; Redding 1967; Moeckel 1972; Benford & Benford 2003; Lubin 2016). By increasing the incident flux upon the light sail versus that caused by the Sun, the acceleration of the sail can be enhanced as required. However, such a proposal invites new challenges, such as (but not limited to) thermal management (Jin et al. 2022), stability within the beam (Manchester & Loeb 2017; Srivastava, Chu, & Swartzlander 2019; Rafat et al. 2022) and actual production and delivery of the input energy. For example, *Breakthrough Starshot* envisages a kilometre-scale, ground-based ~ 100 GW coherent phased-array laser (Worden et al. 2021). These challenges and others have led some to criticise the feasibility of such a system (Katz 2021) and thus motivate us to re-visit the case of a purely Sun-driven sail.

In this work, we introduce and study a new concept which does not rely on directed energy as the primary means of propulsion. We dub this concept as a Torque Accelerator using Radiation from the Sun (TARS) in what follows. In Section 2, we outline the concept. In Sections 3 and 4, we calculate the fluxes and forces experienced by TARS. In Section 5, the spin-up behaviour of TARS is explored, following by a discussion of the nuances of its orbit in Section 6. The achievable velocity of TARS is discussed in Section 7, as well as the impact of payload release on the system itself in Section 8. Section 9 introduces a specific and simplistic design realisation based

upon a uniform ribbon, which we then refine in Section 10 to a more useful design. Finally, we conclude in Section 11, commenting on the possible applications of such a system.

2. CONCEPT

The problem with solar sails is that they tend to move away from the source, thus diminishing their incident flux. To this end, let us start by seeking a solution which can harvest solar radiation without linear translation of the vehicle, at least not initially. The idea is to store solar energy up in some other form, essentially a battery, and then transfer said stored energy into linear kinetic energy once the battery is charged. In this way, one can benefit from the high incident flux found closer to a star.

A basic question is - what form might this battery take? Although several options could be considered, in this paper we focus on an essentially flywheel-like battery. This system is advantageous since it can be charged up directly from solar radiation and then easily transferred to linear kinetic energy. Indeed, it is this transfer from rotational to linear kinetic energy that defines one of the primary safety concerns with flywheels on Earth (Starbuck & Hansen 2009).

The concept is illustrated by considering two light sails attached to one another with a tether, as depicted in Figure 1. Each light sail is identical, with one side coated with a reflective surface and the opposite side coated with a non-reflective surface. The two light sails do not face the same direction, but rather one is rotated 180 degrees around. In this way, the combined system will feel both a linear translational radiation pressure outward, as well as a torque when exposed to approximately plane parallel radiation. The system is similar to the familiar Crookes radiometer toy (Worrall 1982).

The applied torque is utilised to spin-up TARS until the tether approaches break-up tension. At this point, one (or both) sails are detached (or a sail section) and will head off at high speed tangential to the final rotational motion. The light sail(s) will then continue to enjoy thrust from solar radiation in what follows, but crucially the initial high speed provides sufficient momentum to escape our solar system. The concept is attractive since it only involves two light sails and a tether, and is powered by the Sun. In practice, one might consider an initial spin-up phase with directed energy (but far less than 100 GW) or micro-thrusters, since TARS is more stable once rotation is established.

The outlined concept is yet to address the issue of the linear push from solar radiation. We propose that this radially outward force will in general be less than the solar gravitational force in, and thus TARS is still gravitationally bound to the star. However, its orbit will trail that of the Earth if placed at 1 AU, since the radiation pressure effectively reduces the gravitational mass of the Sun (Kezerashvili & Vázquez-Poritz 2009), and thus the orbital speed of TARS. This kind of artificial

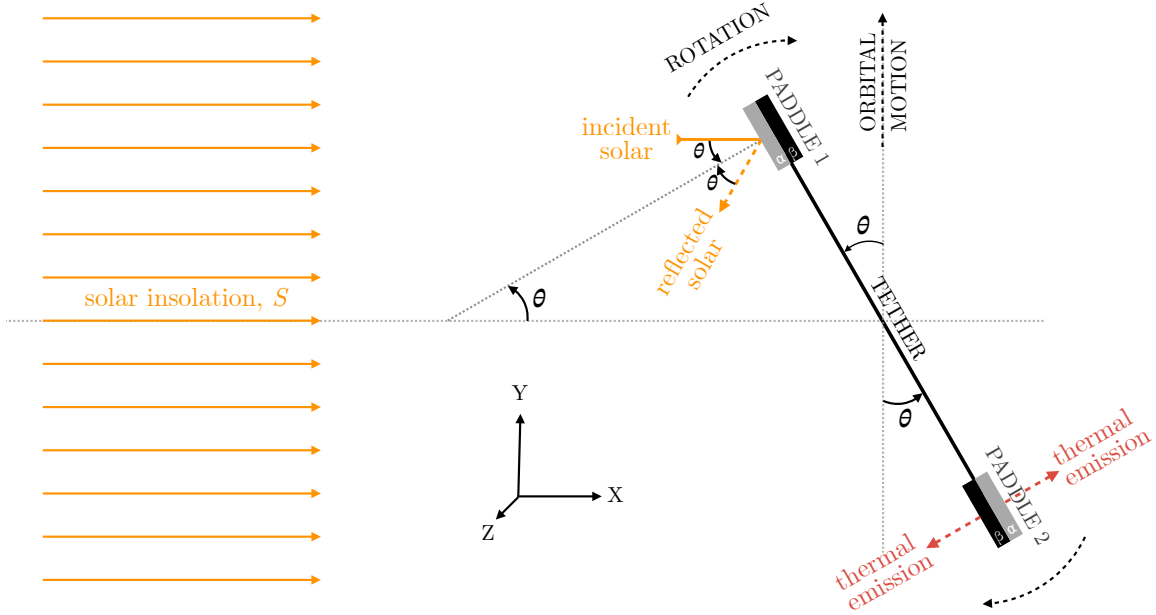


Figure 1. A simplified version of the TARS system. Here, the system comprises of one tether and two paddles, which together are orbiting around the Sun, with an instantaneous velocity vector along the \hat{Y} -axis. Incident solar radiation is largely reflected by the α -surface (the reflective surface) of the paddles, but largely absorbed by the β -surface. This leads to a radiation pressure torque that gradually spins up TARS. Note that both paddles experience both reflection and emission; we only show one of each for the sake of visual clarity in the above.

orbit, dubbed a “quasite” in Kipping (2019), can be placed at any location in our solar system barring gravitational perturbations from nearby planets. In most realistic cases the quasite effect will be fairly small (see Section 10), since although the sails will experience significant radiation pressure, the combined system including the much heavier tether will lead to a higher areal density.

The goals of this paper are not to describe an in-depth engineering blueprint, but rather just outline the concept along with some relevant calculations concerning the theoretical performance. It is not claimed that this system is definitively plausible, merely that it deserves exposition given the enormous challenge and interest in interstellar flight. Although some obvious concerns about feasibility are addressed later, this paper is not intended as a feasibility study of such a system either.

3. FLUXES

Starting from Figure 1, we begin by calculating the incident/emitted fluxes for each paddle surface. In this section, it is initially assumed that the tether does not serve as a substantial radiative surface and can be ignored here, thus corresponding to a narrow tether in projection. Recall that flux is power per unit area, and thus the area of the paddles does not in fact affect the flux calculation, but will enter later when power is calculated. A zoom-in of a paddle showing the various fluxes is illustrated

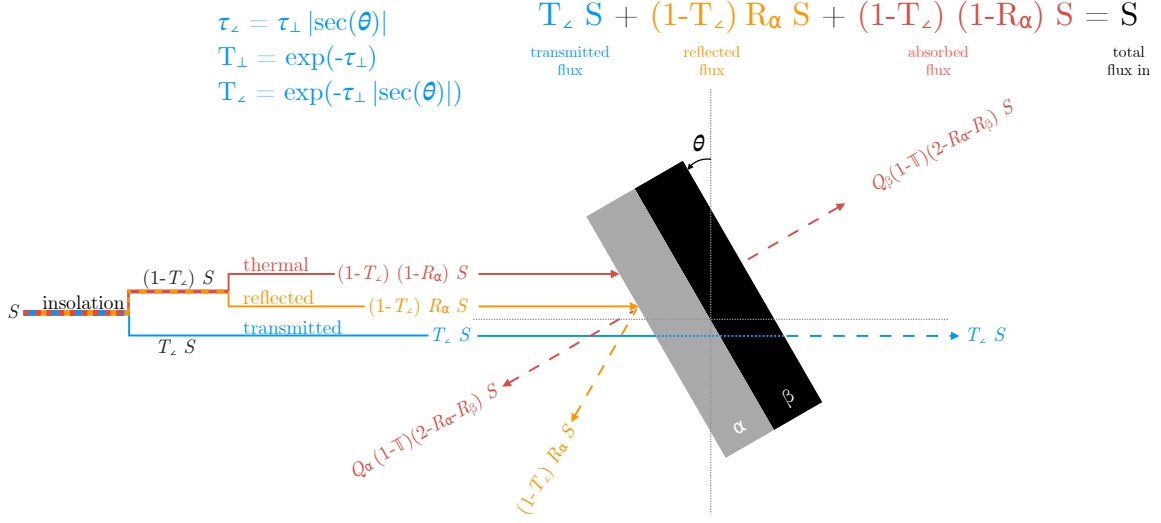


Figure 2. Break-down of fluxes incident (coloured solid) and emitted (coloured dashed) by each surface of one of TARS' paddles. The symbol T is adopted for transmission, R for reflectivity and Q_α to describe heat transport. The term \mathbb{T} is an effective transmission term defined later in Equation (4).

in Figure 2 to guide the reader, where it is assumed that incident flux can either be i) transmitted through the paddle (blue lines), ii) reflected (orange lines), or iii) thermally absorbed/emitted (red).

In Figure 2, incident/absorbed (i.e. incoming) fluxes are shown with solid coloured lines, whereas reflected/emitted (i.e. outgoing) fluxes are shown with dashed coloured lines. The figure denotes a single instant in time, which is certainly reasonable for the reflecting light rays, where it can be safely assumed that the process of reflection occurs in a much shorter timescale than any meaningful motion of the TARS. However, the thermal absorption and then subsequent re-emission cannot be trivially assumed to behave as such, due to thermal lags. To address this, let us calculate the phase-averaged thermal absorption and set this equal to the thermal emission at any one moment in time. In other words, the paddles are assumed to be in thermal equilibrium averaged over their rotation.

To make progress, it is first noted that the instantaneous incident fluxes for phase angles of $-\pi/2 < \theta < \pi/2$ equals²:

$$S = \underbrace{T_z(\theta)S}_{\text{transmitted}} + \underbrace{(1 - T_z(\theta))R_\alpha S}_{\text{reflected}} + \underbrace{(1 - T_z(\theta))(1 - R_\alpha)S}_{\text{absorbed}} \quad (1)$$

where it has been assumed (for simplicity) that the albedo of the α surface, R_α , is the same for all θ here, and hence represents an ideal specular surface. The absorbed flux is highlighted as the final term here. The thermal power absorbed equals this

² for the other angle set, the equation is the same except $\alpha \rightarrow \beta$

flux multiplied by the projected area. Assuming the limiting case of a thin sail, which is certainly desired here, the absorbing area is dominated by the projected area of the paddle's largest surface. If the surface has an area A , then the projected area is $A|\cos\theta|$. Hence, the phase-average absorbed power equals

$$\begin{aligned} \overline{P_{\text{absorbed}}} &= \frac{1}{\pi} \int_{-\pi/2}^{\pi/2} A|\cos\theta|(1 - T_{\angle}(\theta))(1 - R_{\alpha})S \, d\theta \\ &\quad + \frac{1}{\pi} \int_{\pi/2}^{3\pi/2} A|\cos\theta|(1 - T_{\angle}(\theta))(1 - R_{\beta})S \, d\theta. \end{aligned} \quad (2)$$

To make progress, it is necessary to define the transmission function, $T_{\angle}(\theta)$. Let us define the opacity of the paddle for normal incident light as τ_{\perp} . Accordingly, the transmission through the paddle for normal incident light would be $T(\theta = 0) = \exp(-\tau_{\perp})$. The opacity will be proportional to the path length through the paddle, which scales as $\tau_{\perp}|\sec\theta|$. The assumption here is effectively that the thickness layer of the α and β surfaces are comparable, such that even if they have different opacities, the net effect will still scale with $\sec\theta$. Presumably, the opacity should be capped at some upper limit occurring at $\theta = \pm\pi/2$ (when edge-on), since the paddle does not have infinite width. However, both the fact that our paddle is thin and that the transmission here will practically be negligible anyway, means this may be ignored to simplify the integral. Accordingly, Equation (2) becomes

$$\begin{aligned} \overline{P_{\text{absorbed}}} &= \frac{A(1 - R_{\alpha})S}{\pi} \int_{-\pi/2}^{\pi/2} |\cos\theta|(1 - \exp(-\tau_{\perp}|\sec\theta|)) \, d\theta \\ &\quad + \frac{A(1 - R_{\beta})S}{\pi} \int_{\pi/2}^{3\pi/2} |\cos\theta|(1 - \exp(-\tau_{\perp}|\sec\theta|)) \, d\theta. \end{aligned} \quad (3)$$

It was not possible to find a closed-form solution to the above, but after numerically integrating along a grid of τ_{\perp} values, it was found that the integral is well-approximated by $2 - (4/3)e^{-\tau_{\perp}}$, giving

$$\overline{P_{\text{emitted}}} = \overline{P_{\text{absorbed}}} \simeq A(2 - R_{\alpha} - R_{\beta})S \underbrace{\left(\frac{2 - \frac{4}{3}\exp(-\tau_{\perp})}{\pi} \right)}_{=\mathbb{T}}. \quad (4)$$

where the substitution \mathbb{T} absorbs the phase-averaged transmission effects. The above is suitable to within 1% accuracy for all $\tau_{\perp} > 1.34$, which corresponds to transmissions of normal incident light of $T_{\perp} < 26\%$. In general, a desirable paddle will have a lower transmission than this limit and thus this formula is adopted in what follows.

Power is not necessarily emitted equally from both sides of the paddle, due to the different materials in use. To parametrise this, a fraction Q_{α} of $\overline{P_{\text{emitted}}}$ is emitted

from the α -surface, and thus a fraction $Q_\beta \equiv (1 - Q_\alpha)$ is emitted from the β -surface. In line with the thin-paddle approximation, negligible emission comes from the edges of the paddle.

4. FORCES

Equipped with the power incident/emitted off each surface, it is straight-forward to calculate the forces at this point. One simply needs to normalise power by the speed of light.

Splitting the forces into normal and lateral components, one may sum the various terms in the case of an ray incident upon the α -surface of:

$$\begin{aligned}
 F_{\perp,\alpha} = & \underbrace{(A/c) \cos^2 \theta (1 - T_\perp) (1 - R_\alpha) S}_{\text{inc. thml. } \alpha} \\
 & + \underbrace{(A/c) Q_\alpha \mathbb{T} (2 - R_\alpha - R_\beta) S}_{\text{em. thml. } \alpha} \\
 & - \underbrace{(A/c) Q_\beta \mathbb{T} (2 - R_\alpha - R_\beta) S}_{\text{em. thml. } \beta} \\
 & + \underbrace{(A/c) \cos^2 \theta (1 - T_\perp) R_\alpha S}_{\text{inc. refl. } \alpha} \\
 & + \underbrace{(A/c) \cos^2 \theta (1 - T_\perp) R_\alpha S}_{\text{em. refl. } \alpha}. \tag{5}
 \end{aligned}$$

where the direction here is chosen such that a net positive force acts upon the illuminated paddle. The β -surface is effectively the same expression, just swapping the α and β terms over.

Figure 3 shows the various forces vectors and their components. All of the forces are instantaneous forces, that is they depend on the phase angle θ , with the exception of the thermal emission components. For these, it is assumed that the thermal response time is slower than the rotation rate and thus it the temperature of the sail is not rapidly bouncing up and down in phase with the spin, but rather is essentially stable over the rotational timescale. In reality, one might expect some small damped oscillation in temperature in phase with the rotation, but this assumption greatly simplifies our subsequent analysis.

Equation (5) may now be simplified to

$$\begin{aligned}
 F_{\perp,\alpha} = & S(A/c)(1 + R_\alpha) \cos^2 \theta (1 - \exp(-\tau_\perp |\sec \theta|)) \\
 & - S(A/c)(1 - 2Q_\alpha)(2 - R_\alpha - R_\beta) \mathbb{T}. \tag{6}
 \end{aligned}$$

It is briefly noted that lateral forces also exist that in any instant do not cancel due to the asymmetric nature of the paddle albedos. However, averaged over all phases, these forces balance to zero.

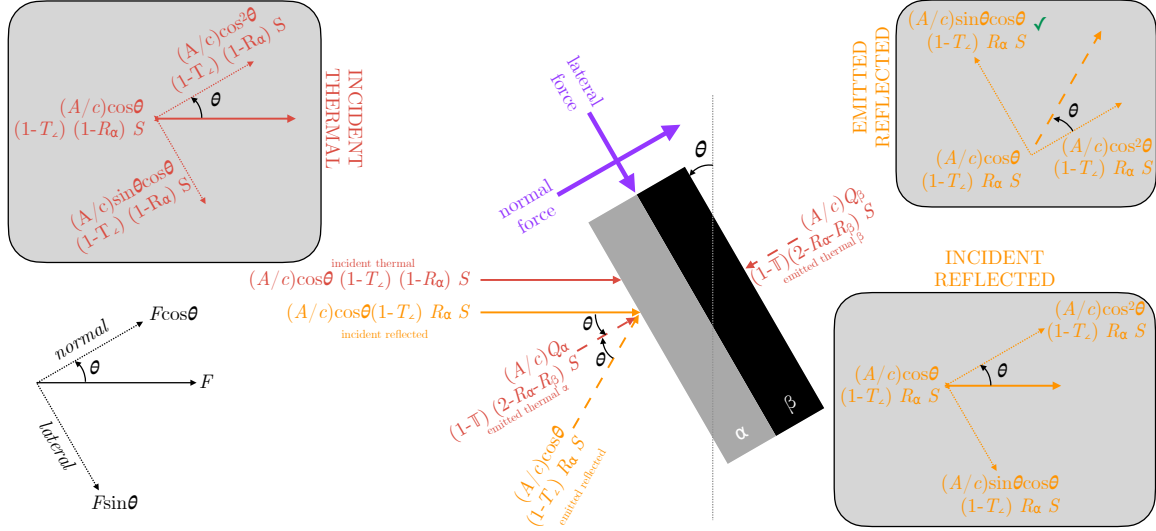


Figure 3. Break-down of the various forces acting upon a paddle when the α -side is Sun-incident. The spin-up of TARS is governed by the normal forces, as well as producing the quasite effect on the structure. The inset boxes show the force components more clearly for the incident thermal (top-left), emitted reflected (top-right) and incident reflected (bottom-right) cases.

TARS is designed to impose $F_{\perp,\alpha} \geq F_{\perp,\beta}$, such that $R_\alpha \gg R_\beta$ and Q_α does not cause a thermal backreaction that out-pushes the reflective radiation pressure. In this way, the force acting on one paddle (the one currently with its α surface under illumination) will exceed that of the other, creating a torque. It is this torque which is used to gradually spin-up TARS to high velocities. In what follows, then, $F_{\perp,\alpha} \geq F_{\perp,\beta}$ is adopted as a design requirement.

5. SPIN-UP

The motion of a rod-like object in a weightless environment being torqued at one end is calculated in Singal (2017). In that work, two scenarios are considered, first, that of a single impulse acting on the end of a rod, and second, that of a continuous force, f . The latter closely resembles our problem except for three differences: i) Singal (2017) consider a uniform rod with moment of inertia $I = ml^2/12$, ii) the force is continuous at all times, unlike our phase-dependent scenario, iii) averaged over all phases, there are no net Cartesian forces acting upon the object.

Point i) will be dealt with later in Section 10, where the design of the sail is explored and the corresponding moment of inertia.

For points ii) and iii), one can correspond the forces depicted in Figure 3 to that presented in Singal (2017) as follows. Consider a phase position $-\pi/2 < \theta < \pi/2$, such that paddle 1 has its α -surface under illumination, whereas for paddle 2 its β -surface is sunlit. This is the phase position shown in Figure 1. Paddle 1 thus feels a normal force of $F_{\perp,\alpha}$, acting to torque TARS in a clockwise sense (as depicted in Figure 1), whereas paddle 2 feels an opposing normal force of $F_{\perp,\beta}$, acting in the

counter-clockwise sense. Since $F_{\perp,\alpha} \geq F_{\perp,\beta}$, then there is a net-torque in the clockwise direction, F_R , given by

$$F_R = F_{\perp,\alpha} - F_{\perp,\beta}. \quad (7)$$

Accordingly, one may consider that both paddles are being pushed by a force of $F_{\perp,\beta}$, but paddle 1 experiences an extra push on top of that of F_R . Because both paddles are being pushed by $F_{\perp,\beta}$, the centre-of-mass of the system will experience a force, F_C , of

$$F_C = 2F_{\perp,\beta}. \quad (8)$$

In phase position $\pi/2 < \theta < 3\pi/2$, paddle 2 now has its α -surface under illumination and thus experiences the greater force. Here, the centre-of-mass still experiences a net force F_C , but now paddle 2 experiences the net force F_R . However, given the symmetry of our system, this is equivalent to paddle 1 experiences the force still, in terms of the resulting torques.

One may now equate this setup to that of [Singal \(2017\)](#). Ignoring the phase-dependent forces for the moment, the setups are equivalent modulo that TARS experiences an additional net force on its centre-of-mass. This force is trying to accelerate TARS radially away from the Sun. As discussed already, such an outward acceleration is problematic since it will, if left unchecked, cause TARS to recede from the Sun and thus decrease the incident flux. The proposed solution to this problem is to invoke the quasite scheme, which will be discussed in further detail later in [Section 6](#).

This just leaves the issue of a phase-varying force. As TARS spins up, these become of increasingly less concern. At high speed, the motion will asymptotically approach that of the mean forces. A similar situation is described in [Singal \(2017\)](#) with respect to the centre-of-mass's motion, which experiences uneven nudges initially, but at rapid rotational rates stabilises to a fixed point in velocity-space. Accordingly, the rotational motion of TARS will follow that of [Singal \(2017\)](#) except their f is our phase-averaged F_R ($\overline{F_R}$) and the moment of inertia will be distinct. In the limit of $\tau_{\perp} \rightarrow \infty$ (i.e. zero transmission through the paddles), one finds

$$\lim_{\mathbb{T} \rightarrow 0} \overline{F_R} = 2\epsilon_R \left(\frac{AS}{c} \right). \quad (9)$$

where ϵ_R is defined as a scalar governing the quality of TARS' design, here set to

$$\epsilon_R = \frac{1}{4\pi} \left(16Q_{\alpha}(2 - R_{\alpha} - R_{\beta}) - 16 + 8(R_{\alpha} + R_{\beta}) + \pi(R_{\alpha} - R_{\beta}) \right). \quad (10)$$

One might imagine a perfect system to correspond to $R_\alpha \rightarrow 1$, $R_\beta \rightarrow 0$ and $Q_\alpha \rightarrow 1$, yielding $\epsilon_R = (8 + \pi)/(4\pi) = 0.887$. However, ϵ_R takes a maximal value of $4/\pi$ for $R_\alpha = R_\beta = 0$ and $Q_\alpha = 1$ - a perfect thermal thruster. In the case of an ideal reflector but no thermal thrust ($R_\alpha \rightarrow 1$, $R_\beta \rightarrow 0$ and $Q_\alpha \rightarrow 1/2$), one obtains $\epsilon_R \rightarrow 1/4$. After initial spin-up, the angular rotation rate will now increase linearly with respect to time (Singal 2017) at a rate of

$$\dot{\omega} = \frac{\overline{F_R} \delta}{I}, \quad (11)$$

where δ is the distance from where the force F_R acts to the centre of TARS. In the case of a homogenous ribbon of material, $\delta = L/4$ (where L is the end-to-end length of TARS), $I = ML^2/12$ and $M = 2\Sigma A$ (since the two paddles connect together in this simplified case), thus yielding

$$\dot{\omega} = 3 \frac{\epsilon_R S}{c \Sigma L}. \quad (12)$$

If the orbit of TARS was strictly circular, then S is a constant, but in general an eccentric orbit will experience time-variable insolation. In cases where TARS will take many years to charge to full capacity, the insolation term can be replaced with the time-averaged insolation per orbit, \bar{S} . From Méndez & Rivera-Valentín (2017), the time-averaged insolation is

$$\bar{S} = S_\oplus \frac{1}{(a/\text{AU})^2} \frac{1}{\sqrt{1-e^2}}. \quad (13)$$

Adopting this, one can write that the linear speed of TARS, after a time t , will be

$$v = 3t \left(\frac{\epsilon_R S_\oplus}{c \Sigma} \right) \frac{1}{(a/\text{AU})^2} \frac{1}{\sqrt{1-e^2}}. \quad (14)$$

Some example values for the time to reach $v = 10$ km/s are provided in Table 1. The last column shows the case of a highly eccentric orbit, such that perihelion is two Solar radii and aphelion is 1 AU, corresponding to $a = 0.5047$ AU and $e = 0.9816$, which increases \bar{S} by a factor of 20.55. Remarkably, the charge times are quite modest, especially for the very low areal density cases, indicating that a sail of such extreme minimal thickness is not strictly required.

6. ORBIT

An issue that has yet to be discussed is that of the outward radial force exerted on TARS' centre-of-mass, F_C , and how this affects the orbit. As before, let us first define the phase-averaged value this force takes, as

Table 1. Some example values of the time to reach a useful velocity using Equation (11). The term t_1 is the time to reach $v = 10$ km/s for $a = 1$ AU and $e = 0$ with $R_\alpha = 1$, $R_\beta = 0$ and $Q_\alpha = 1/2$. The time t_2 is the same except assuming a high-performance (but sub-optimal) $\epsilon_R = (8 + \pi)/(4\pi)$. The time t_3 is the same as t_2 , except for an eccentric orbit with $r_{\text{peri}} = 2 R_\odot$ and $r_{\text{ap}} = 1$ AU (a 20.5-fold increase in average insolation).

Sail	Σ [g m ⁻²]	t_1	t_2	t_3
<i>Lightsail2</i> (Spencer et al. 2021)	143	13.3 years	3.8 years	9.5 weeks
<i>Sunjammer</i> (Eastwood et al. 2015)	45.5	4.2 years	1.2 years	3.0 weeks
<i>Breakthrough Starshot</i> (Worden et al. 2021)	0.2	6.8 days	1.9 days	2.2 hours

$$\lim_{T \rightarrow 0} \overline{F_C} = 2\epsilon_C \left(\frac{AS}{c} \right), \quad (15)$$

where

$$\epsilon_C = \frac{1}{2\pi} \left(\pi(1 + R_\beta) - 4(2Q_\alpha - 1)(2 - R_\alpha - R_\beta) \right). \quad (16)$$

In general, one expects $\overline{F_C} > 0$ corresponds to an outward radial force away from the energy source. Curiously, for extreme choices of Q_α the sign reverses. Such a case is likely not realisable without a heat pump of some kind, since it corresponds to the paddle thermally emitting almost exclusively on a single side, implying a strong temperature gradient. The same behaviour can of course occur for conventional sails too, if they absorb a significant amount of flux and then primarily re-radiate on the side facing away from the Sun.

In the typical case of a positive outward force, $\overline{F_C}$ is seemingly a major issue since it would push TARS away from its current location like a solar sail, thereby diminishing the incident radiation. To avoid this, it is proposed to place TARS in a sub-Keplerian, quasite orbit (Kipping 2019). Quasites are the middle-ground between a statite (Forward 1993) and a conventional satellite. A statite has extremely low areal density (~ 0.77 g/m²), such that the outward force of radiation pressure is sufficient to balance gravitational forces. A quasite is not so light, but still experiences sufficient radiation pressure that a meaningful portion of the Sun’s gravitational attractive force is still balanced. In this way, it needs to orbit the Sun, like a satellite does, in order to avoid in-fall. However, the speed of its orbit need not be Keplerian, but rather it is sub-Keplerian.

For a conventional solar sail, Kezerashvili & Vázquez-Poritz (2009) showed that the kinematics of a quasite sail are well-described with Keplerian motion, except that the mass of the Sun is effectively reduced from $M_\star \rightarrow \tilde{M}_\star$, where

$$\tilde{M}_\star = M_\star - \frac{\eta L_\star}{2\pi c G \Sigma}. \quad (17)$$

In the above, L_\star is the stellar luminosity, Σ is the areal density of the quasite. Kezerashvili & Vázquez-Poritz (2009) don't explicitly define η but describe that $\eta = 1$ corresponds to a perfectly reflective sail and $\eta = 1/2$ is a perfectly absorbing sail.

To relate η to \overline{F}_C , consider what \overline{F}_C would be if replaced TARS with a simple solar sail orthogonal to the incident radiation. In the case of no transmission, one finds

$$\lim_{T_\perp \rightarrow 0} \overline{F}_C = \frac{AS}{c} 2(R + Q(1 - R)), \quad (18)$$

where Q is the ratio of heat emitted from the Sun-ward side to the space-ward side. In the limit of a perfect reflector, what Kezerashvili & Vázquez-Poritz (2009) call $\eta = 1$, one obtains

$$\lim_{R \rightarrow 1} \lim_{T_\perp \rightarrow 0} \overline{F}_C = 2 \frac{AS}{c}. \quad (19)$$

For the perfect absorber, $\eta = 1/2$, instead one finds

$$\lim_{Q \rightarrow 1/2} \lim_{R \rightarrow 0} \lim_{T_\perp \rightarrow 0} \overline{F}_C = \frac{AS}{c}. \quad (20)$$

From this, one can see that η is simply defined as

$$\eta = \frac{\overline{F}_C}{2AS/c}. \quad (21)$$

Accordingly, in our case, $\eta = \epsilon_C$ and thus

$$\tilde{M}_\star = M_\star - \frac{\epsilon_C L_\star}{2\pi c G \Sigma}. \quad (22)$$

If TARS remains bound to the Sun, then one requires that the last term does not exceed M_\star .

7. PAYLOAD RELEASE

As TARS spins up, the ends eventually approach some desired target velocity, v_{targ} , at which point the payload is released. Beyond this speed, there will also be a critical velocity, v_{crit} , where TARS tears itself apart from centrifugal forces.

In the case where TARS is on a circular orbit, the moment of release need not be precisely when $v = v_{\text{targ}}$, but rather can be at a specific orbital phase position instead. In this way, the direction of the payload can be controlled - although it is fated to always lie in the plane of TARS' orbit and thus careful consideration of the orbit will be required. Through detailed calculation, it may be possible to synchronise the

orbital phase position of the release with the moment when target velocity is reached, thus allowing one to engineer v_{targ} as close to v_{crit} as is dared. There will certainly be some control here since TARS may experience an initial spin-up phase and/or could be further fine-tuned with directed energy upon the paddles.

It is instructive to consider the potential of TARS to reach interstellar escape velocity, v_{esc} , given by

$$v_{\text{esc}} = \sqrt{\frac{2G\tilde{M}_\star}{r}}, \quad (23)$$

where r is the radial distance from the Sun. Note how the familiar M_\star term is replaced with \tilde{M}_\star (Equation 22) due to the quasite effect, which essentially captures how the payload enjoys an outward radiation pressure during its exodus from our solar system. In the limit of a circular orbit, the required target velocity to escape our solar system will be

$$\lim_{e \rightarrow 0} v_{\text{targ,req}} = (\sqrt{2} - 1) \sqrt{\frac{G\tilde{M}_\star}{r}}, \quad (24)$$

and for $r = 1 \text{ AU}$ this demands a 12.3 km/s rotational velocity using *Lightsail2*-like parameters with $\epsilon_C = 1$. This highlights how it is challenging, but feasible, to engineer a TARS system which can go interstellar, a topic discussed in greater depth in Section 10. Even without interstellar speeds, TARS is potentially still useful for interplanetary missions, but let us briefly consider how the system could be modified to reach interstellar space in what follows. One obvious possibility to increase r , since

$$v_{\text{targ,req}} \propto \frac{1}{\sqrt{r/\text{AU}}}. \quad (25)$$

For example, placing TARS at or beyond Mars' orbit would just about achieve escape velocity with $v_{\text{targ}} = 10.0 \text{ km/s}$, using *Lightsail2*-like properties. However, since $v_{\text{targ}} \propto r^{-2}$ (see Equation 14), this more than doubles the spin-up time, although given the times in Table 1 this is perhaps perfectly acceptable. Of course, TARS would have to be first be manoeuvred to or constructed in such an orbit, which is clearly less practical.

An alternative is for TARS to have an eccentric orbit to begin with. This obviously requires some extra energy to move the vehicle into such an orbit, but has some considerable benefits in terms of payload speed. A wide array of orbits could be considered here, but for the sake of demonstrating its advantages, consider an orbit with perihelion of $20 R_\odot$ and aphelion 1 AU, such that $a = 0.5465 \text{ AU}$ and $e = 0.8298$ - which is less extreme than achieved by NASA's *Parker* probe. Releasing the payload at perihelion, with the same parameters otherwise as used earlier, yields

$$v_{\text{targ,req}} = 6.0 \text{ km/s}. \quad (26)$$

In other words, the critical velocity is approximately halved thus greatly reducing the engineering requirements on the system. Effectively, TARS here is exploiting the Oberth effect (Blanco & Mungan 2019). The kinetic energy of TARS is maximised at perihelion, and hence applying a delta-v at this point maximises the energy gain.

For the suggested orbit, the perihelion temperature would peak at 913 K on the β -paddles, which although is too high for Mylar, is below the melting point of metals such as aluminium (934 K) and beryllium (1560 K) which could be polished for the reflective coatings. With this orbit, $\bar{S} = 6S_{\oplus}$ and thus we still enjoy decreased charge times compared to the nominal circular 1 AU case. In what follows, the rest of this study considers strictly circular orbits at 1 AU. Although this is not optimal for maximal speeds, it is optimal in terms of launch energetics thereby focussing on the most viable realisation in a practical sense.

8. BACKREACTION & RECHARGING

After the payload release, the angular momentum of TARS will be affected. The effect is estimated in what follows, using the simplifying assumption of a uniform density ribbon (thin rectangular plate). Different designs will of course yield different results, but the below provides intuition about the expected outcomes.

Consider the system has an angular momentum of $J = I\omega$ just before release, where $I = \frac{1}{12}ML^2$. For the payload release, imagine an end of the paddle being removed of length ΔL and mass ΔM , such that the new moment of inertia becomes $I' = \frac{1}{12}(M - \Delta M)(L - \Delta L)^2$.

At the same time, the payload itself carries away an angular momentum $r \times p$, where $p = v\Delta M = \omega r\Delta M$ and r is the distance of the payload's barycentre from the rotation axis, given by $r = (L/2 - \Delta L/2)$. Thus, the new angular momentum of the system is

$$\begin{aligned} J' &= \frac{1}{12}ML^2\omega - r^2\Delta M\omega, \\ &= \frac{1}{12}ML^2\omega - (L/2 - \Delta L/2)^2\Delta M\omega, \end{aligned} \quad (27)$$

which can be equated to the new momenta of inertia and angular velocity as

$$\frac{1}{12}(M - \Delta M)(L - \Delta L)^2\omega' = \frac{1}{12}ML^2\omega - (L/2 - \Delta L/2)^2\Delta M\omega. \quad (28)$$

And thus the new angular velocity, relative to the old, can be written as

$$\frac{\omega'}{\omega} = \frac{1 - 3\Delta m(1 - \Delta l)^2}{(1 - \Delta m)(1 - \Delta l)^2}, \quad (29)$$

which uses the substitutions $\Delta m = \Delta M/M$ and $\Delta l = \Delta L/L$. Since uniform density is assumed, then $\Delta m = \Delta l$ and thus

$$\frac{\omega'}{\omega} = \frac{1 - 3\Delta m(1 - \Delta m)^2}{(1 - \Delta m)^3}, \quad (30)$$

which is greater than unity for all $\Delta m > 0$ and reaches a maximum value of 5 for $\Delta m \rightarrow 1/2$. Since the velocity of the ends is given by $\omega' L'$, then the new velocity can be shown to satisfy

$$\frac{v'}{v} = \frac{1 - 3\Delta m(1 - \Delta m)^2}{(1 - \Delta m)^2}, \quad (31)$$

which is less than unity (as perhaps our intuition might expect) for all positive Δm , taking a limit of 5/2 when $\Delta m \rightarrow 1/2$. For payloads of relatively small mass, one finds

$$\frac{v'}{v} = 1 - \Delta m + \mathcal{O}[\Delta m^2]. \quad (32)$$

If the payload was released close to v_{crit} , which is independent of M or L for a uniform density ribbon, then TARS will slow down to a sub-critical velocity after release. Afterwards, TARS will continue to feel a torque, although the centre-of-force has now shifted due to the asymmetrical release at just one end. In principle then, it should recharge back up to critical velocity and could be used to launch another payload. Indeed, a series of payloads could be released in this way. To ensure the rotational axis does not shift and potentially lead to unstable rotation, a double payload could be released, one from each end (even if one of these is a ballast payload). This modification changes Equation (31) to

$$\frac{v'}{v} = \frac{1 - 6\Delta m(1 - \Delta m)^2}{(1 - 2\Delta m)^2}, \quad (33)$$

or simply

$$\frac{v'}{v} = 1 - 2\Delta m + \mathcal{O}[\Delta m^2]. \quad (34)$$

This notion of a series of payload releases separated by a recharge time is attractive since the recharge time will be a small fraction of the initial charge time, making TARS more cost-efficient by releasing multiple probes. Indeed, using Equation (14), the recharge time will be

$$\Delta t \simeq \frac{2}{3} \Delta m v_{\text{crit}} \left(\left(\frac{\epsilon_R S_{\oplus}}{c \Sigma} \right) \frac{1}{(a/\text{AU})^2} \frac{1}{\sqrt{1-e^2}} \right)^{-1} \quad (35)$$

Given the constraint that payloads must be released in the same plane, a possible strategy is to release a series of micro-probes to the same destination, forming a daisy-chain physically separated by $\sim v_{\text{crit}} \Delta t$. Such a system could allow for the low-power probes to maintain a communication line back to Earth.

9. UNIFORM RIBBON

In what follows, let us consider what is arguably the simplest version of TARS - a homogenous ribbon. Here, there is no tether, the paddles extend and mate at the midpoint. The midpoint is identified as the point where the coatings change, from α to β values. More optimal designs surely exist, as discussed in Section 10, but the uniform ribbon is attractive for simplifying the calculations in what follows.

9.1. Critical Velocity

First, let us derive the critical velocity at which the ribbon will fail due to the centrifugal forces exceeding the tensile strength. The ribbon (really a rectangular plate) is defined to have a length L , width W , thickness t , density ρ and tensile strength σ .

Consider an element of the ribbon of length of dx of the ribbon, located a distance x from the centre and rotating at an angular velocity ω . The centrifugal force experienced by this element will be

$$dF = \rho W t dx \omega^2 x. \quad (36)$$

The tension, \mathcal{T} , acting at a distance x from the centre can be found by integrating the above from position x to $L/2$, such that the tension is the sum of the centrifugal forces acting outward beyond the point x :

$$\begin{aligned} \mathcal{T}(x) &= \int_x^{L/2} \rho W t \omega^2 x \, dx, \\ &= \frac{1}{8} (L^2 - 4x^2) W t \rho \omega^2. \end{aligned} \quad (37)$$

At $x = L/2$, we can see that the tension falls to zero (i.e. $\mathcal{T}(L/2) = 0$), as expected for the boundary conditions of the problem. At the midpoint, the structure experiences a maximum tension of

$$\mathcal{T}(0) = \frac{1}{8} L^2 W t \rho \omega^2. \quad (38)$$

The failure load is defined as the tensile strength multiplied by the cross-sectional area, and hence here equals σWt . Equating this to $\mathcal{T}(0)$ and re-arranging, one obtains

$$\omega_{\text{crit}}^2 = \frac{8\sigma}{\rho L^2}, \quad (39)$$

and thus

$$v_{\text{crit}} = \sqrt{2} \sqrt{\frac{\sigma}{\rho}}. \quad (40)$$

9.2. Material

A key design requirement is to maximise the specific strength i.e. σ/ρ . Graphene is the most promising material in this regard with a density of 2.3 g m^{-3} and tensile strength of 130 GPa. However, graphene is difficult to produce in large continuous sections and thus the following considers instead carbon nanotube (CNT) sheets, with a density of 1.6 g m^{-3} and tensile strength up to 20 GPa. Although CNT sheets have a specific strength five times worse than graphene, they are a more mature product and one which is currently available on the market.

For the thickness of TARS, one might apply a thin optical coating on either side of CNT sheets, of at least 10 nm. Given that the optical coatings will have negligible tensile strength, they dilute the overall tensile strength. To overcome this, it is proposed to make the CNT sheets much thicker than 10 nm, such that the bulk properties asymptotically approach that of pure CNT sheets. Of course, the more mass that is added, the longer the spin-up time and thus a possible compromise is a CNT sheet of order of a micron thickness, which is already in widespread production.

For the α surface, a possible choice is a thin (~ 10 nm or 35 atoms thick) coating of nanostructured silver to deliver low transmission and high reflectance (~ 0.9) due to localised surface plasmon resonances (Kuzminova et al. 2019). Other options might include silver or beryllium with dielectric coatings (such as SiO_2 , TiO_2 or HfO_2) or doping the coating (Atwater et al. 2018). Such a coating would be painted onto the CNT sheets using processes such as physical vapour deposition (Mattox 1998) or chemical vapour deposition (Ohring 2002). Aluminium and lithium should be avoided if aphelion $\lesssim 20 R_\odot$ is planned, due to their lower melting points.

For the β surface, a possible choice is a thin (~ 10 nm or 71 atoms thick) coating of titanium nitride (Patsalas et al. 2015). Even this thin layer would have negligible transmission and deliver low optical reflectance (~ 0.3).

As presented, this ribbon has no payload but one could certainly imagine adding payloads of low mass compared to the ribbon at the ends without significant performance losses. Rather than go into the minutiae of such a proposal, let us instead move onto an improved design which is more interesting to consider in detail.

10. TAPERED RIBBON

10.1. *Payload-Free Scenario*

To begin, consider the case of a payload-free tapered ribbon. In the previous section, the critical angular velocity was calculated by setting the tension at the midpoint to be equal to the failure load. However, if one moves further along the ribbon, the tension decreases and thus the ribbon is unnecessarily wide. Thus, one should be able to improve performance by gradually narrowing the width of the ribbon towards the ends - a tapered ribbon.

Let us split the ribbon up into N equi-length segments from $x = 0$ to $x = L/2$, assigning each one a unique width W_i and segment length $(L/2)/n$. Imposing symmetry reflects this configuration from $x = 0$ to $x = -L/2$. The bounds around each segment follow $(i/n)(L/2)$ from $i = 0$ (the midpoint) to $i = n$ (the end). One may define a general $\mathcal{W}(x)$ piecewise function which returns W_i when x corresponds to a distance (from the midpoint) within the i^{th} segment.

Beginning at the midpoint, the critical angular velocity is again found by balancing the tension and the failure load - a solution labelled as $\omega_{\text{crit},1}$. One may then move along up to $i = n$ solving the following equation each time for ω :

$$\int_x^{L/2} \rho \mathcal{W}(x') t \omega^2 x' dx' = \sigma \mathcal{W}(x) t. \quad (41)$$

Let us set $\omega_{\text{crit},i} = \omega_{\text{crit},i-1}$ and solve for W_i , working backwards from $i = n$ to $i = 2$ (W_1 is treated as a design parameter), which yields the following recursive solution

$$W_i = \frac{2(n+1-i)}{2n-1} W_{i-1}. \quad (42)$$

Accordingly, in terms of W_1 only, these solutions become

$$W_i = \frac{\prod_{j=2}^i 2(n+1-j)}{(2n-1)^{i-1}} W_1. \quad (43)$$

Applying these solutions, one finds, for all $i \in [1, n]$:

$$\omega_{\text{crit},i} = \frac{n}{\sqrt{2n-1}} \times \underbrace{\left(2\sqrt{2} \frac{\sqrt{\sigma}}{\sqrt{\rho L}} \right)}_{\text{uniform solution}}. \quad (44)$$

Hence, this tapering scheme allows one to arbitrarily increase ω_{crit} (at the expense of ever larger structures).

Each segment has a width W_i , length $(L/2)/n$ and uniform thickness t . The area of each segment is thus $A_i = W_i(L/2)/n$. Given that the assumption of uniform density, ρ_{bulk} , then the mass elements are $M_i = A_i t \rho_{\text{bulk}}$. As before, there is still no payload but a scheme for including payload is presented in what follows.

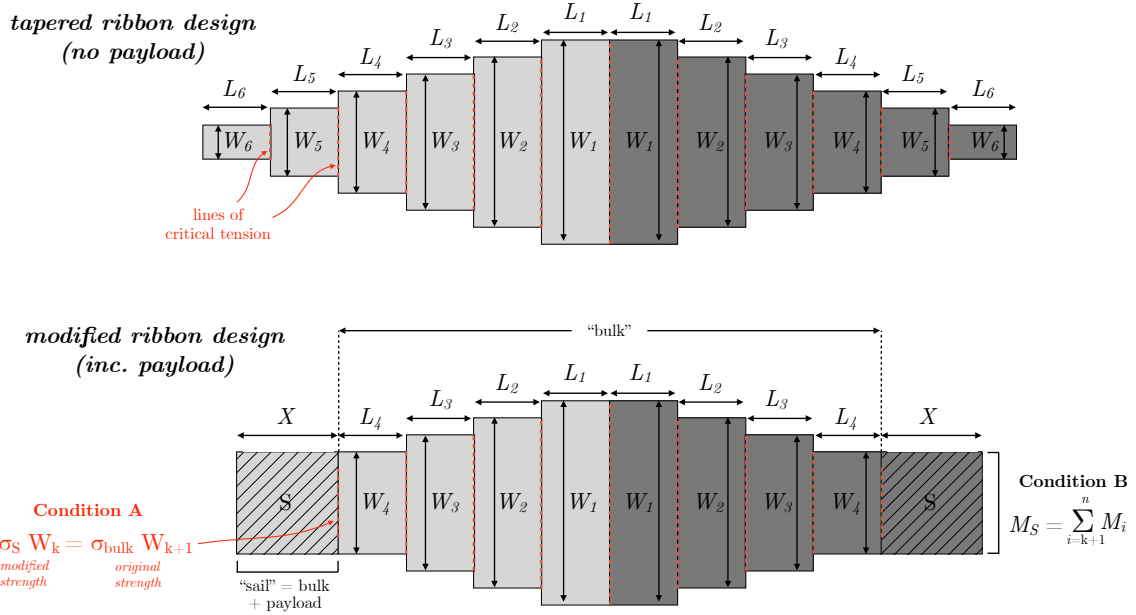


Figure 4. The tapered ribbon design of TARS. Top: The case of a tapered ribbon ($n = 6$) with no payload and made of a homogeneous material (the bulk). The α and β sides are shaded appropriately. Moving away from the rotation axis, the segments become of ever smaller widths, W_i , since the tension reduces and thus less tensile strength is required to resist failure. The red lines depict points of critical tension when TARS reaches ω_{crit} . Bottom: A modification of the above where the $k = 4$ inner segments are kept but those beyond are replaced with a sail containing the payload. The sail has poorer tensile strength due to the payload and thus the width is inflated to provide the necessary additional tensile strength. Condition A is the criterion to avoid the sail breaking off before ω_{crit} , and condition B conserves mass.

10.2. Adding Payload

Consider replacing segments $k + 1$ to n with a single segment that includes the same basic materials, a core of CNT sheets with the same optical coatings, but also includes a thin payload layer. For simplicity, the thickness of this new section is considered to be equal to that of the rest of TARS (the “bulk”), which means the thickness of CNT sheets (and thus specific strength) is less in this end section to accommodate the payload. The proposal is depicted in Figure 4.

As the payload-containing segment will ultimately be released and fly as a sail, it will be referred to as the “sail” segment in what follows. Due to the diminished specific strength of the sail, to avoid failure one requires that $W_S > W_{k+1}$ to provide sufficient tensile strength. This work chooses to set $W_S = W_k$ to create a continuous joint. This increased cross-sectional area provides added tensile strength to compensate for the weaker specific strength of the composite sail material. Since the thickness of the sail and bulk are matched, then to avoid failure one requires condition A of

$$\begin{aligned}\sigma_S W_k &= \sigma_{\text{bulk}} W_{k+1}, \\ \sigma_S &= \sigma_{\text{bulk}} \frac{2(n-k)}{2n-1}.\end{aligned}\tag{45}$$

where the second line uses Equation (42). By volumetric mixing, $t_{\text{bulk}}\sigma_S = t_{\text{payload}}\sigma_{\text{payload}} + (t_{\text{bulk}} - t_{\text{payload}})\sigma_{\text{bulk}}$, which allows one to re-write condition A as:

$$1 - \frac{t_{\text{payload}}}{t_{\text{bulk}}} = \frac{2(n-k)}{2n-1}.\tag{46}$$

One may use this condition to calculate the mean density of the sail component, since again by volumetric mixing one has

$$\rho_S = \left(\frac{t_{\text{payload}}}{t_{\text{bulk}}}\right)\rho_{\text{payload}} + \left(1 - \frac{t_{\text{payload}}}{t_{\text{bulk}}}\right)\rho_{\text{bulk}}.\tag{47}$$

Next, let us impose a condition B - that the mass of the sail equals the cumulative mass of the removed sections (meaning that that TARS's total mass is unaffected by our modification), such that

$$\begin{aligned}M_S &= \sum_{i=k+1}^n M_i, \\ \rho_S W_k X &= \sum_{i=k+1}^n W_i \frac{L}{2n} \rho_{\text{bulk}}.\end{aligned}\tag{48}$$

This ensures the general formula for the critical angular velocity found earlier (Equation 44) remains true. The above may be re-arranged to give a solution for X as a function of L , a solution that will be used shortly to define the final dimensions of the system.

The spin-up of TARS will now be governed by the moment of inertia and centre-of-pressure location, following Equation (11). The centre-of-pressure distance, δ , is simply the centre-of-area since the TARS has a uniform optical coating, and is thus

$$\delta = \frac{XW_k d_S + \sum_{i=1}^k W_i \frac{L}{2n} d_i}{XW_k + \sum_{i=1}^k W_i \frac{L}{2n}}\tag{49}$$

where $d_i = (2i-1)L/(4n)$ and $d_S = ((kL)/(2n)) + (X/2)$ are the distances of the relevant sections from the axis of rotation. The moments of inertia are calculated using

$$\begin{aligned}
I_X = & 2 \sum_{i=1}^k \int_{x=(i-1)(L/2)/n}^{i(L/2)/n} \int_{y=-W_i/2}^{W_i/2} \int_{z=-t/2}^{t/2} \rho_{\text{bulk}}(y^2 + z^2) dx dy dz \\
& + 2 \int_{x=k(L/2)/n}^{X+k(L/2)/n} \int_{y=-W_k/2}^{W_k/2} \int_{z=-t/2}^{t/2} \rho_S(y^2 + z^2) dx dy dz
\end{aligned} \tag{50}$$

and similarly for I_Y and I_Z . These are particularly important for not only the spin-up time but also designing a system that does not risk tumbling (Goldstein 1980). The axis of rotation is along the Y -direction and thus one must ensure that the intermediate moment of inertia is not I_Y , which in practice means designing a system such that $I_Y < I_X < I_Z$.

The velocity of the sail, as it approaches the critical angular rotational speed, is

$$v_{\text{crit}} = d_S \omega_{\text{crit}}. \tag{51}$$

If released tangential to the orbital motion, the total speed of the sail will additive to this extra speed. However, because TARS is a quasite, the orbital speed is sub-Keplerian, given by

$$v_{\text{orb}} = \sqrt{\frac{2}{r} - \frac{1}{a}} \sqrt{G} \sqrt{M_\star - \frac{\epsilon_C L_\star}{2\pi c G \Sigma_{\text{eff}}}}, \tag{52}$$

where Σ_{eff} is the total mass of TARS divided by its area. To maximise radial escape, the sail will orient such that the α -side only is Sun-facing, thus modifying the quasite effect. The escape velocity from the Sun is then given by Equation (23) but with $\epsilon_C = (1 + R_\alpha)/2$.

10.3. Numerical Examples

This work does not attempt a comprehensive optimisation of the design parameters, but instead this subsection explores the effect of some of the parameters to provide guidance on the plausible capabilities.

To set the scale of the system, this work sets $W_k = 0.1$ m as a test case, yielding a sail with an area of 0.01 m² - comparable to the dimensions of a modern smart phone. For the thickness, let us adopt a 6 μm thick layer of CNT sheets and a 20 nm total thickness of optical coating. One may now experiment with different choices of n and k and solve for the final system parameters. In all cases, a circular orbit is assumed, as well as $S = S_\oplus$ (i.e. an Earth-trailing orbit). Further, it is assumed that $Q_\alpha = 1/2$, $R_\alpha = 0.9$ and $R_\beta = 0.3$.

Consider first the simplest case of $n = 2$ and $k = 1$. In this case, one finds $v_{\text{crit}} = 3.6$ km/s for which the spin-up time is 263.9 days. TARS has an effective areal density of 10.9 g/m² whereas the sail component is 13.1 g m², comprised of a payload thickness

of 2007 nm. This configuration is unstable to tumbling and also lacks the ability to go to interstellar, with $v_{\text{orb}} + v_{\text{crit}} = 32.0 \text{ km/s}$, 7.8 km/s shy of the escape speed. With a length of 0.8 m and a W_1 width of 0.1 m, the structure has a high aspect ratio.

To optimize the system, consider increasing to $n = 50$, providing more fine control over the location of the sail component. Exploring from $k = 1$ to $k = 49$, it was found that stable configurations occur for $k \geq 18$ and interstellar-capable configurations for $k \geq 24$, as shown in Figure 5. At large n , such as that used here, TARS shows enormous dynamic range in scale as a function of k , spanning 21 orders-of-magnitude in mass, 18 orders-of-magnitude in W_1 and nearly 4 orders-of-magnitude in length. Large k choices lead to unreasonably large systems and thus it is desirable to select the smallest k which is both stable and interstellar, here $k = 24$.

The $n = 50$ and $k = 24$ design has $W_1 = 62.7 \text{ m}$ with a payload thickness of 2860 nm, which should be sufficient for a thin computer chip. The system achieves $v_{\text{crit}} = 12.1 \text{ km/s}$, $v_{\text{orb}} + v_{\text{crit}} = 40.4 \text{ km/s}$ and has a Sun escape velocity of 40.0 km/s. We estimate a charge time of $\omega_{\text{crit}}/\dot{\omega} = 351.1$ days. With a total mass of a 1.6 kg and being constructed from materials already in widespread production, this provides a possible example of a realisable interstellar sail.

Notably, the sail component here has mean density of 14.6 g/m^2 (total area is 164.4 m^2), which is an order-of-magnitude heavier than a statite sail that would balance radiation pressure with gravitational acceleration (Forward 1993). Thus, TARS could achieve interstellar flight using existing materials, solar radiation pressure only and with an thickness an order-of-magnitude greater than that of TARS-free solar sail. This highlights the advantages of the system as a possible stepping stone technology to future sails.

11. DISCUSSION

This work has explored the possibility of using the Sun’s radiation to spin-up a thin structure in space with the ultimate goal of releasing a payload at high velocities. Although much of this work has set the goal of reaching escape velocity from our solar system, such a system is of course useful for interplanetary missions too.

To our knowledge, this idea has not been previously explored in the literature and thus much of this paper derives the basic equations governing the flux, forces, orbit, charging time, critical velocity and design constraints. For the sake of conciseness, this paper is not intended as an exhaustive examination of the technical feasibility of such a system, nor is it claimed that it is definitively cost-effective, practical or feasible - although this analysis finds no clear objections.

With existing materials, a 1-2 kg TARS can eject smart-phone sized sails into interstellar space with less than a year’s worth of charge-up time - powered by the Sun. The final velocities are by no means relativistic and thus our analysis suggests such a system cannot satisfy the goals of *Breakthrough Starshot* (Parkin 2018), who seek $0.2c$ (although in what follows we discuss some mechanisms of increasing the final

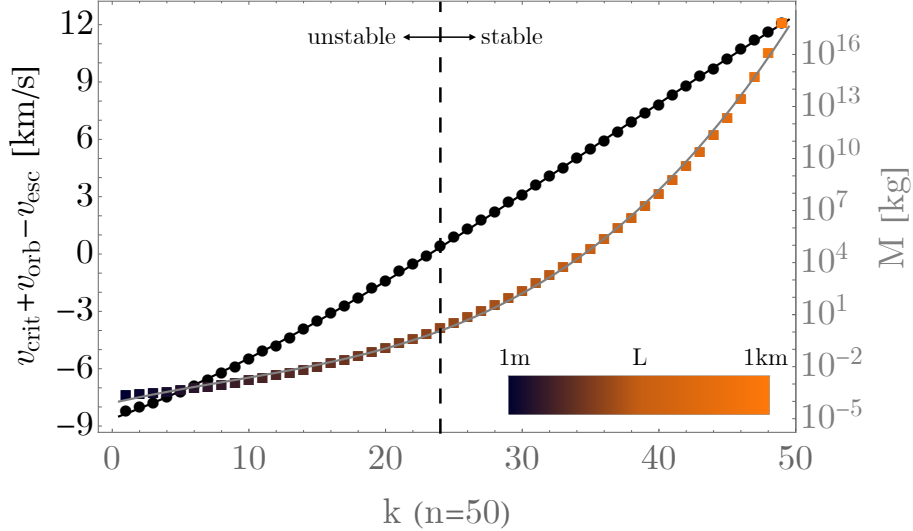


Figure 5. Black circles and black line depicts the payload’s velocity at release minus the escape velocity from our solar system (left y -axis) as a function of k , a design parameter for the tapered ribbon design. Rust-coloured squares and grey line depicts TARS’s mass as a function of k (right y -axis), where one can see the rapid ballooning of scale as k increases. The colours denote the length of the system. The vertical line delineates the region of stability versus non-stability.

speed). The system perhaps best lends itself to cases where such high speeds are not required and, be it for cost-driven or legal-constraints, the use of \sim GW lasers is prohibitive. The system is also in principle multi-use, as discussed in Section 8. Ultimately, this paper is an intellectual exercise - it is the author’s belief that the landscape of possible solutions should be investigated and publicly disseminated to provide us with the context of how best to proceed.

11.1. Going Faster

Although TARS can achieve escape velocity from our solar system using the Sun’s radiation pressure alone, the ejection speeds are comparatively slow and thus it is worth discussing methods by which greater speeds could be attained. The previously discussed Oberth effect is an example of this (see Section 6), but may not be cost-effective given the need to first transfer into an eccentric Sun-grazing orbit.

An obvious improvement would be introduced by increasing the specific strength of the materials used. In particular, the promise of large, high-grade graphene sheets would lead to significant improvements. For example, setting $n = 20$ and $k = 12$ for a $5 \mu\text{m}$ thick system with a $0.1\text{m} \times 0.1\text{m}$ sail, we find that an $L = 8.2\text{m}$ graphene TARS ($\sigma_{\text{bulk}} = 120 \text{ GPa}$) would reach $v_{\text{crit}} + v_{\text{orb}} - v_{\text{esc}} = 9.4 \text{ km/s}$ after 867 days of charging (and would be stable). Briefer charge times would be possible by modifying the orbit, as discussed in Section 5.

Another improvement would be to perform the same trick as used by previous interstellar probes i.e. gravity assists. Velocity boosts of up to $\sim 10 \text{ km/s}$ are routinely

possible, which can be stacked for planetary alignments to produce significant extra speed (Dodd 2020).

A third possibility is to treat TARS as merely an initial launch phase followed by acceleration with laser pressure (Marx 1966; Redding 1967; Forward 1984). In many ways, this echoes the approach of *SpinLaunch* - a private company attempting to use a centrifuge to deliver 1-2 km/s of initial launch speed followed by conventional chemical rocket systems to escape the Earth's gravity well (Niederstrasser 2022).

A fourth approach is the idea of artificially increasing the tensile strength of the material via the use of a restoring force generated by the vehicle itself, which is briefly discussed in the next subsection.

11.2. Charged Paddles

TARS is ultimately limited by the tensile strength of known materials. One possible way to increase v_{crit} further would be to apply an equal and opposite electrostatic charge to each tip, q . In what follows, a brief and approximate estimation of the impact of this is explored. The opposite charges would lead to a rotating dipole of magnitude

$$m = \frac{1}{2}qL^2\omega. \quad (53)$$

A rotating magnetic dipole generates a magnetic field, which in principle could be useful for other purposes such as a space weather protection or controlling plasmas. A rotating dipole radiates electromagnetic waves with a power given by

$$\begin{aligned} P_{\text{rad}} &= \frac{\mu_0\omega^4 m^2}{6\pi c^3}, \\ &= \frac{\mu_0 q^2 L^4 \omega^6}{24\pi c^3}. \end{aligned} \quad (54)$$

The total power incident upon TARS is given by Equation (4). Equating these two, the maximum charge that could be used before the system would bleed power is

$$q^2 = \frac{48\pi c^3 AS(2 - R_\alpha - R_\beta)}{\pi\mu_0 L^4 \omega^6} \quad (55)$$

The electrostatic force bringing these charges together will thus be

$$\begin{aligned} F &= \frac{1}{4\pi\epsilon_0} \frac{q^2}{L^2}, \\ &= \frac{12c^5 AS(2 - R_\alpha - R_\beta)}{\pi\omega^6 L^6}. \end{aligned} \quad (56)$$

This competes with the centrifugal force of the rotating system. Equating to that force and re-arranging for $v = \omega(L/2)$ yields

$$v = \left(\frac{3c^5 SL}{32\pi \Sigma} \right)^{1/8},$$

$$\simeq 1000 \text{ km/s} \left(\frac{S}{S_{\oplus}} \right)^{1/8} \left(\frac{L}{100 \text{ m}} \right)^{1/8} \left(\frac{\Sigma}{10 \text{ g/m}^2} \right)^{-1/8} \quad (57)$$

where it has been assumed that $R_{\alpha} = 1$ and $R_{\beta} = 0$ for simplicity. Whilst certainly not comparable to the goal of *Breakthrough Starshot's* $0.2c$, a speed of 0.3% the speed of light would quite an improvement from previous systems, reaching Proxima Centauri in just over a millennia.

ACKNOWLEDGEMENTS

Special thanks to donors to the Cool Worlds Lab, without whom this kind of research would not be possible: Douglas Daughaday, Elena West, Tristan Zajonc, Alex de Vaal, Mark Elliott, Stephen Lee, Zachary Danielson, Chad Souter, Marcus Gillette, Tina Jeffcoat, Jason Rockett, Tom Donkin, Andrew Schoen, Reza Ramezankhani, Steven Marks, Nicholas Gebben, Mike Hedlund, Leigh Deacon, Ryan Provost, Nicholas De Haan, Emerson Garland, The Queen Road Foundation Inc, Scott Thayer, Frank Blood, Ieuan Williams, Xinyu Yao & Axel Nimmerjahn.

REFERENCES

- Atwater H. A., Davoyan A. R., Ilic O., Jariwala D., Sherrott M. C., Went C. M., Whitney W. S., et al., 2018, *NatMa*, 17, 861. doi:10.1038/s41563-018-0075-8
- Benford J., Benford G., 2003, *AIPC*, 664, 303. doi:10.1063/1.1582119
- Blanco P. R., Mungan C. E., 2019, *PhTea*, 57, 439. doi:10.1119/1.5126818
- Dodd S., 2020, AGUFMSH01, 2020, SH019-01
- Eastwood J. P., Kataria D. O., McInnes C. R., Barnes N. C., Mulligan P., 2015, *Wthr*, 70, 27. doi:10.1002/wea.2438
- Forward R. L., 1984, *JSpRo*, 21, 187. doi:10.2514/3.8632
- Forward R. L., 1993, "Statite: Spacecraft That Utilizes Light Pressure and Method of Use", US patent 5183225
- Goldstein H., 1980, *Classical Mechanics*, 2nd edn. Addison-Wesley, Reading, MA
- Jin W., Li W., Khandekar C., Orenstein M., Fan S., 2022, arXiv, arXiv:2206.05383
- Katz J. I., 2021, *RNAAS*, 5, 61. doi:10.3847/2515-5172/abf124
- Kezerashvili R. Y., Vázquez-Poritz J. F., 2009, *PhLB*, 675, 18. doi:10.1016/j.physletb.2009.03.058
- Kipping D., 2019, *RNAAS*, 3, 91. doi:10.3847/2515-5172/ab2fdb
- Kuzminova, K., Solar, P., Kus, P., Kylian, O., 2019, *Journal of Nanomaterials*, 2019, 1. doi:10.1155/2019/1592621
- Lebedev P., 1901, "Untersuchungen über die Druckkräfte des Lichtes", *Annalen der Physik*, Series 4 6, 433
- Lubin P., 2016, *JBIS*, 69, 40
- Manchester Z., Loeb A., 2017, *ApJL*, 837, L20. doi:10.3847/2041-8213/aa619b
- Marx G., 1966, *Natur*, 211, 22. doi:10.1038/211022a0

- Mattox D. M., 1998, Handbook of Physical Vapor Deposition (PVD) Processing, 1st edn. William Andrew Publishing, Norwich, NY.
- Méndez A., Rivera-Valentín E. G., 2017, *ApJL*, 837, L1.
doi:10.3847/2041-8213/aa5f13
- Moeckel W. E., 1972, *JSpRo*, 9, 942.
doi:10.2514/3.30415
- Nichols E. F., Hull G. F., 1903, *ApJ*, 17, 315. doi:10.1086/141035
- Niederstrasser, C.G., 2022. The small launch vehicle survey: A 2021 update (The rockets are flying). *Journal of Space Safety Engineering*, 9(3), 341-354. doi:10.1016/j.jsse.2022.07.003
- Ohring M., 2002, *Materials Science of Thin Films: Deposition and Structure*, 2nd edn. Academic Press, San Diego, CA.
- Parkin K. L. G., 2018, *AcAau*, 152, 370.
doi:10.1016/j.actaastro.2018.08.035
- Patsalas P., Kalfagiannis N., Kassavetis S., 2015, *Materials*, 8, 3128.
doi:10.3390/ma8063128
- Powers R. B., Coverstone V. L., 2001, *JAnSc*, 49, 269.
doi:10.1007/BF03546322
- Rafat M. Z., Dullin H. R., Kuhlmeier B. T., Tuniz A., Luo H., Roy D., Skinner S., et al., 2022, *PhRvP*, 17, 024016.
doi:10.1103/PhysRevApplied.17.024016
- Redding J. L., 1967, *Natur*, 213, 588.
doi:10.1038/213588a0
- Singal A. K., 2017, arXiv, arXiv:1708.05062.
doi:10.48550/arXiv.1708.05062
- Spencer D. A., Betts B., Bellardo J. M., Diaz A., Plante B., Mansell J. R., 2021, *AdSpR*, 67, 2878.
doi:10.1016/j.asr.2020.06.029
- Srivastava P. R., Chu Y.-J. L., Swartzlander G. A., 2019, *OptL*, 44, 3082. doi:10.1364/OL.44.003082
- Starbuck, J. M. & Hansen, J. G., 2009, Office of Scientific and Technical Information (OSTI), 975070.
doi:10.2172/975070
- Tsiolkovsky K. E., 1968, K. E. Tsiolkovsky Selected Works, compiled by V. N. Sokolosky, MIR Publishers (Moscow), English Translation
- Weiss R. F., Pirri, A. N., & Kemp, N. H. 1979, *Astronautics and Aeronautics*, 17, 50
- Worden S. P., Green W. A., Schalkwyk J., Parkin K., Fugate R. Q., 2021, *ApOpt*, 60, H20. doi:10.1364/AO.435858
- Worrall J., 1982, *SHPSA*, 13, 133.
doi:10.1016/0039-3681(82)90023-1
- Zander F. 1964, Problems of flight by jet propulsion: Interplanetary flights, NASA Technical Translation F-147